Inorganic Chemistry

Article

pubs.acs.org/IC

Structural and Spectroscopic Characterization of Iron(II), Cobalt(II), and Nickel(II) *ortho*-Dihalophenolate Complexes: Insights into Metal−Halogen Secondary Bonding

Timothy E. Machonkin,*[,†] Monica D. Boshart,[†] Jeremy A. Schofield,[†] Meghan M. Rodriguez,[‡] Katarzyna Grubel,[‡] Dalia Rokhsana,[†] William W. Brennessel,[‡] and Patrick L. Holland*[,‡,§]

[†]Department of Chemistry, Whitman College, Walla Walla, Washington 99362, United States

[‡]Department of Chemistry, University of Rochester, Rochester, New York 14627, United States

Supporting Information

ABSTRACT: Metal complexes incorporating the tris(3,5-diphenylpyrazolyl)borate ligand (Tp^{Ph2}) and *ortho*-dihalophenolates were synthesized and characterized in order to explore metal−halogen secondary bonding in biorelevant model complexes. The complexes $Tp^{Ph2}ML$ were synthesized and structurally characterized, where M was Fe(II), Co(II), or Ni(II) and L was either 2,6-dichloro- or 2,6-dibromophenolate. All six complexes exhibited metal−halogen secondary bonds in the solid state, with distances ranging from 2.56 Å for the Tp^{Ph2}Ni(2,6-dichlorophenolate) complex to 2.88 Å for the Tp^{Ph2}Fe(2,6-dibromophenolate) complex. Variable temperature NMR spectra of the Tp^{Ph2}Co(2,6-dichlorophenolate) and Tp^{Ph2}Ni(2,6-dichlorophenolate) complexes showed that rotation of the phenolate, which requires loss of the secondary bond, has an activation barrier of ∼30 and ∼37 kJ/mol, respectively. Density functional theory calculations support the presence of a barrier for disruption of the metal−halogen interaction during rotation of the phenolate. On the other hand, calculations using the spectroscopically calibrated angular overlap method suggest essentially no contribution of the halogen to the ligand-field splitting. Overall, these results provide the first quantitative measure of the strength of a metal−halogen secondary bond and demonstrate that it is a weak noncovalent interaction comparable in strength to a hydrogen bond. These results provide insight into the origin of the specificity of the enzyme 2,6-dichlorohydroquinone 1,2-dioxygenase (PcpA), which is specific for *ortho*-dihalohydroquinone substrates and phenol inhibitors.

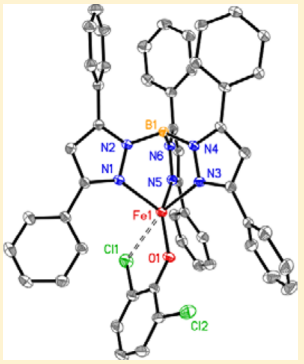

INTRODUCTION

Pentachlorophenol is a toxic xenobiotic compound that was introduced in the early twentieth century as a pesticide and is still used today as a wood preservative.[1] Although the use of pentachlorophenol has been restricted, it is still commonly found in the environment. Interestingly, in the short time pentachlorophenol has been present in the environment, the bacterium *Sphingobium chlorophenolicum* has evolved to fully degrade it.[2] The enzyme 2,6-dichlorohydroquinone 1,2-dioxygenase (PcpA) provides the key step in this degradation process, using O_2 to cleave the aromatic ring of 2,6-dichlorohydroquinone.[3−5]

The structure of PcpA is similar to a well-studied class of enzymes,[6] the catechol extradiol dioxygenases (EDOs),[7,8] as confirmed by a recent crystal structure.[9] Both are mononuclear nonheme iron(II)-containing dioxygenases with similar active site structures. They are also functionally comparable: while PcpA cleaves the aromatic ring of hydroquinones, EDOs cleave the aromatic ring of catechols. Despite of the similarities between PcpA and the EDOs, they differ greatly in their behavior toward halogenated substrates. In general, EDOs are not active toward chlorinated substrates, and instead such compounds are potent mechanism-based inactivators.[10−13] In contrast, the native substrate of PcpA is a chlorinated compound, 2,6-dichlorohydroquinone.

Many aspects of the mechanism of PcpA and the basis for its substrate specificity remain unknown. Kinetic studies have shown that PcpA exhibits a strong selectivity toward *ortho*-dihalohydroquinone substrates and phenol inhibitors over the corresponding methyl-substituted versions.[14] The origin of this unique specificity is currently unknown, and there are not yet crystallographic data for PcpA interacting with substrates or inhibitors. In order to identify the most important factors, model complexes would be valuable tools to explore the possible binding modes of substrates and inhibitors to metal ions like the one in the PcpA active site. In particular, we anticipated that iron(II) complexes with *ortho*-halophenols could demonstrate bonding factors that explain the preference of PcpA for halogenated substrates and inhibitors.

In our previous work, the supporting ligand was *cis,cis*-1,3,5,-tris(*E*)-(tolylideneimino)-cyclohexane (TACH-*o*-tolyl), a tridentate facially coordinating ligand. The resulting [(TACH-*o*-tolyl)FeL]$^+$ complexes, where L was 2-chloro-, 2,6-dichloro-, or 2,6-dibromophenolate, each exhibited short interactions

Received: June 17, 2014
Published: August 28, 2014

   dx.doi.org/10.1021/ic501424e | *Inorg. Chem.* 2014, 53, 9837−9848

between the halogen substituent and the iron(II) center, ranging from 2.84 to 3.12 Å.[15] These short interactions are classified as "metal−halogen secondary bonds," which are formally defined as halocarbon complexes having a halogen-metal distance considerably below the sum of their van der Waals radii but longer than the metal-halide bond length.[16−20] On the basis of nuclear quadrupole resonance (NQR) spectroscopy results, Wulfsberg proposed the criterion that the metal−halogen distance must be shorter than the average metal-halide distance plus 1 Å.[19] Using the average four-coordinate Fe(II)-chloride bond length of 2.30 Å,[21] all of the $[(TACH\text{-}o\text{-}tolyl)FeL]^+$ complexes meet this criterion for metal−halogen secondary bonding. This shows that an *ortho*-halophenolate can form an *additional interaction* with the iron(II) center. This direct interaction between the halogen and the metal could increase the binding affinity of halogenated substrates and inhibitors to PcpA and thus contribute to the unusual substrate specificity of this enzyme.

However, the postulation of a metal−halogen secondary bond based on distance alone is necessarily tentative. Metal−halogen secondary bonds are relatively rare,[15−19,22−27] and there are few techniques capable of detecting these bonds other than X-ray crystallography and NQR.[17−20] Consequently, the characteristics of these secondary bonds are in need of greater understanding. In particular, to our knowledge there are no quantitative studies of the strength of this interaction, nor is it clear to what extent the halogen can be classified as a true "ligand" to the metal center. More detailed studies of TACH-*o*-tolyl complexes were not possible because the supporting ligand was unstable with respect to isomerization and dissociation.[15] Therefore, we chose a tris(pyrazolyl)borate (Tp) ligand[28−30] as a more stable tridentate supporting group for the synthesis of metal *ortho*-halophenolate complexes. To provide a similar level of steric bulk to the TACH-*o*-tolyl ligand, the ligand tris(3,5-diphenylpyrazolyl)borate (Tp^{Ph2}) was selected for the present study.[31] A series of Fe(II)-phenolate complexes have been reported previously with the ligand tris(3,5-diisopropylpyrazolyl)borate (Tp^{iPr2}), including a 2,6-dichlorophenolate complex (although it was not structurally characterized).[32] Ni(II)-2,6-diisopropylphenolate complexes have been reported with the ligands tris(3,5-dimethylpyrazolyl)borate (Tp*) and tris(3-phenyl-5-methylpyrazolyl)borate.[33] In addition, Fiedler and co-workers have reported a series of $Tp^{Ph2}FeL$ complexes where L is a either one of several hydroquinonates or 2-amino-4,6-di-*tert*-butylphenolate.[34−36] Here we report the synthesis and characterization of a series of metal *ortho*-dihalophenolate complexes, and examine the nature of the metal−halogen interaction using crystallography, spectroscopy, and computational analysis.

RESULTS

Synthesis and Structural Characterization. The bulky tridentate ligand Tp^{Ph2} was synthesized according to literature procedures.[31] While the active site in PcpA contains iron(II), the *ortho*-dihalophenolate complexes reported herein contain iron(II), cobalt(II), and nickel(II) in order to explore trends with respect to the metal ion and gain deeper insight into metal−halogen bonding.

The starting complex $Tp^{Ph2}FeBr$ was prepared in a similar manner to the previously reported $Tp^{iPr2}FeCl$ complex and characterized by ^1H NMR spectroscopy.[32] Likewise, $Tp^{Ph2}CoCl$ and $Tp^{Ph2}NiBr$ were prepared according to the literature procedures and characterized by ^1H NMR spectroscopy.[37,38] To each of these complexes was added the sodium salt of either 2,6-dichlorophenol (2,6-dcp) or 2,6-dibromophenol (2,6-dbp) (see Scheme 1). In each case, the reactions were performed

Scheme 1. Synthesis of Compounds 1 (M = Fe(II), X = Cl, Y = Br), 2 (M = Fe(II), X = Br, Y = Br), 3 (M = Co(II), X = Cl, Y = Cl), 4 (M = Co(II), X = Br, Y = Cl), 5 (M = Ni(II), X = Cl, Y = Br), and 6 (M = Ni(II), X = Br, Y = Br)

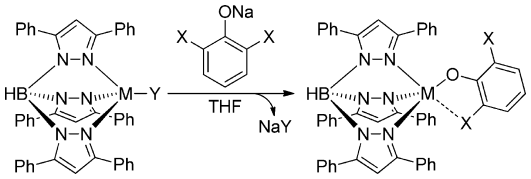

anaerobically in THF. Reaction of $Tp^{Ph2}FeBr$ with these sodium salts yielded colorless $Tp^{Ph2}Fe(2,6\text{-dcp})$ (**1**) and $Tp^{Ph2}Fe(2,6\text{-dbp})$ (**2**) in 71% and 76% yield, respectively. Reactions of $Tp^{Ph2}CoCl$ with 2,6-dcp and 2,6-dbp gave purple $Tp^{Ph2}Co(2,6\text{-dcp})$ (**3**) and $Tp^{Ph2}Co(2,6\text{-dbp})$ (**4**) in 74% and 80% yield, respectively. Reactions of $Tp^{Ph2}NiBr$ with 2,6-dcp and 2,6-dbp gave orange $Tp^{Ph2}Ni(2,6\text{-dcp})$ (**5**) and $Tp^{Ph2}Ni(2,6\text{-dbp})$ (**6**) in 58% and 71% yield, respectively. Complexes **3**−**6** were air-stable, while compounds **1** and **2** were handled under anaerobic conditions.

Crystallographic analysis of **1**−**6** gave structures that are shown in Figure 1. Complexes **1**, **2**, **5**, and **6** cocrystallized with disordered solvent. Selected crystallographic data for **1**−**6** are summarized in Table 1. For all six complexes, the bond angles reveal a distorted five-coordinate geometry. In a trigonal bipyramidal description, N3 and X1 are the axial positions, and O1, N1, and N5 are the equatorial positions. The axial M−N3 distance is slightly longer than the equatorial M−N distances, and all the M−N distances decrease in the order Fe > Co > Ni, in accordance with the trend in metal ion radii.[21] For each of the six complexes, the sum of the angles of the equatorial ligands is nearly 360° (354−360°), and the axial-to-equatorial bond angles are ∼90° for both N3−M−N_{eq} (86°−93°) and X1−M−N_{eq} (92°−101°), supporting the description of a trigonal bipyramidal geometry. However, the complexes exhibit varying levels of distortion toward a square pyramidal geometry, with one O1−M−N_{eq} bond angle significantly larger than the other (116°−126° versus 132°−150°), which in turn leads to τ values[39] that range from 0.32 and 0.33 for complexes **1** and **5** up to a value of 0.72 for **3**. Distortions from an ideal trigonal bipyramidal geometry are found for the N3−M−O1 bond angle (94°−109°) and the X1−M−O1 bond angle (73°−81°). In a square-pyramidal description, N1 (N5 in **2** and **3**) is the axial position. The N_{ax}−M−N_{eq} angles are 90°−96°, the N_{ax}−M−X1 angles are 86°−100°, and the N_{eq}−M−X1 angles are 166°−176°. The most notable distortion away from a square pyramidal description again occurs for the N−M−O1 angles, in which the N_{ax}−M−O1 angle is much greater than 90° and the N_{eq}−M−O1 angle is much less than 180°.

All six complexes exhibited metal−halogen secondary bonding, as judged using Wulfsberg's geometric criterion.[19] The metal−halogen distances decreased in the order Fe > Co > Ni, ranging from 2.89 Å for **2** to 2.56 Å for **5**, in accordance with ionic radii;[21] however, there was no consistent pattern for the M−Cl versus M−Br distance compared to halogen size.[40,41] The M−O1−$C46_{phen}$ bond angle decreased in the same trend,

dx.doi.org/10.1021/ic501424e | Inorg. Chem. 2014, 53, 9837−9848

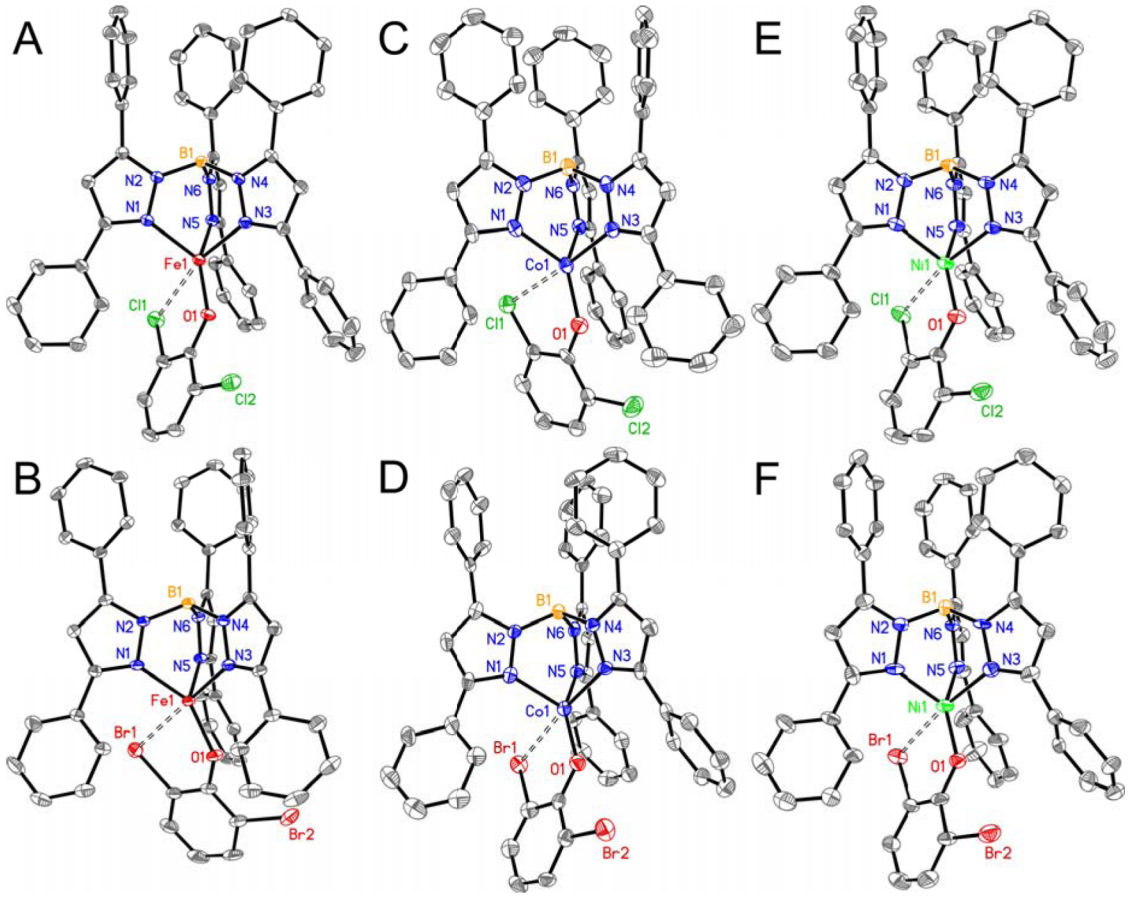

Figure 1. Solid state structures of **1**–**6**, with thermal ellipsoids shown at 50% probability. Hydrogen atoms are omitted for clarity. The metal–halogen secondary bond in each complex is indicated by a dashed line. A, $Tp^{Ph2}Fe$(2,6-dcp) (**1**); B, $Tp^{Ph2}Fe$(2,6-dbp) (**2**); C, $Tp^{Ph2}Co$(2,6-dcp) (**3**); D, $Tp^{Ph2}Co$(2,6-dbp) (**4**); E, $Tp^{Ph2}Ni$(2,6-dcp) (**5**); F, $Tp^{Ph2}Ni$(2,6-dbp) (**6**).

Table 1. Selected Crystallographic Data for $Tp^{Ph2}Fe$(2,6-dcp) (1), $Tp^{Ph2}Fe$(2,6-dbp) (2), $Tp^{Ph2}Co$(2,6-dcp) (3), $Tp^{Ph2}Co$(2,6-dbp) (4), $Tp^{Ph2}Ni$(2,6-dcp) (5), and $Tp^{Ph2}Ni$(2,6-dbp) (6)

	1	2	3	4	5	6
			Bond Lengths (Å)			
M–N1	2.1135(17)	2.089(2)	2.038(3)	2.045(4)	2.0319(16)	2.024(6)
M–N3	2.1250(16)	2.136(2)	2.088(3)	2.092(5)	2.0387(15)	2.043(6)
M–N5	2.0973(16)	2.103(2)	2.036(3)	2.062(5)	2.0348(15)	2.027(6)
M–O1	1.8995(14)	1.8997(17)	1.885(3)	1.882(4)	1.9035(13)	1.905(5)
M–X1	2.8618(8)	2.8853(5)	2.8325(12)	2.8105(10)	2.5601(6)	2.6846(12)
			Bond Angles (deg)			
O1–M–N1	119.13(6)	143.31(8)	132.45(12)	119.52(18)	116.67(6)	118.5(2)
O1–M–N5	147.67(7)	121.48(8)	125.66(12)	144.10(18)	149.52(6)	146.7(2)
N1–M–N5	92.34(6)	93.37(8)	95.63(12)	95.34(18)	93.50(6)	94.3(2)
N3–M–O1	98.34(6)	102.25(8)	108.90(12)	98.14(17)	93.95(6)	95.9(2)
N3–M–N1	92.21(6)	86.32(8)	91.47(12)	91.75(18)	93.48(6)	93.4(2)
N3–M–N5	86.85(6)	91.93(8)	90.15(12)	88.37(18)	88.05(6)	87.2(2)
X1–M–O1	72.95(4)	76.22(6)	75.03(9)	78.39(12)	80.14(4)	80.67(15)
X1–M–N1	100.76(4)	91.86(6)	86.80(9)	93.24(12)	96.82(4)	94.06(16)
X1–M–N5	95.34(4)	93.4(6)	86.18(9)	92.28(13)	92.74(4)	92.02(16)
N3–M–X1	166.73(5)	174.53(6)	175.77(9)	174.88(13)	169.60(5)	172.58(17)
$M–O1–C46_{phen}$	133.66(13)	133.01(17)	130.1(3)	130.8(4)	125.79(13)	129.1(5)
$C47_{phen}–X1–M$	92.45(7)	88.35(9)	91.35(14)	88.64(19)	94.92(7)	89.9(2)
			Torsion Angles (deg)			
$M–O1–C46_{phen}–C47_{phen}$	−13.7(3)	14.0(4)	15.4(5)	−14.3(8)	−5.3(3)	−8.1(10)
$N3–M–O1–C46_{phen}$	−177.32(17)	172.2(2)	163.5(3)	−169.0(5)	176.33(15)	−179.8(6)
			τ values			
	0.32	0.52	0.72	0.51	0.33	0.43

dx.doi.org/10.1021/ic501424e | *Inorg. Chem.* 2014, 53, 9837–9848

to accommodate the shorter M−X1 distance. The $C47_{phen}$−X1−M bond angles were all ~90° (87°−94°), consistent with what has been seen before for metal−halogen secondary bonding[15,18,19] and with what is known about the anisotropic charge density of the halogen.[42] In all complexes, the phenyl ring is nearly coplanar with the N3−M−O1 plane, as shown by the N3−M−O1−$C46_{phen}$ and M−O1−$C46_{phen}$−$C47_{phen}$ torsion angles, thus allowing for the maximum interaction between the halogen substituent and the metal center.

^{1}H NMR Spectroscopic Studies. Complexes **1**−**6** were analyzed by ^{1}H NMR spectroscopy at room temperature (Figure S1). These spectra were consistent with the presence of the desired Tp^{Ph2} M(2,6-dihalophenolate) complexes in solution, and the large shifts indicate that the complexes are paramagnetic. Based upon integrations and expected patterns of hyperfine shifts, the pyrazole H4 and the meta and para protons of the phenolate could be readily identified and assigned (Table 2). Some of the resonances, particularly the Tp^{Ph2} phenyl protons in the nickel(II) complexes, were not resolved and therefore could not be assigned.

Table 2. Selected Room Temperature ^{1}H NMR Data for Complexes 1−6

complex	pyrazole H4	phenolate meta	phenolate para
	Chemical Shifts (ppm)		
1	57.9	54.2	−23.7
2	58.4	54.3	−26.2
3	68.1	35.2	−34.1
4	67.4	37.3	−34.7
5	72.4	29.0	−25.2
6	71.3	28.0	−25.3

In the solid state structures, these complexes show approximate C_s symmetry, and the meta protons of the phenolate are inequivalent. However, in the room-temperature ^{1}H NMR spectra of all six complexes the three arms of the Tp^{Ph2} ligand are equivalent, as are the meta protons of the phenolate ring. Thus, rapid rotation of the phenolate ring about the M−O1 and/or O1−$C46_{phen}$ bonds is occurring on the NMR time scale. This, in turn, indicates that the metal−halogen secondary bond is not maintained in solution at room temperature. The same result was observed in the previously reported TACH-*o*-tolyl complexes.[15] In the case of [(TACH-*o*-tolyl)Fe(2,6-dcp)]$^+$, ^{1}H NMR spectra recorded at temperatures down to −40 °C did not yield decoalescence of the phenolate meta proton signals.

The greater solubility of the present complexes in a wider range of solvents allowed the acquisition of NMR spectra at lower temperatures. Complexes **3** and **5** were selected for variable temperature NMR (VT-NMR) studies. Figure 2A shows the ^{1}H NMR spectra of **3** in CD_2Cl_2 at temperatures from +20 to −89.5 °C. The line width (full width at half-maximum) of the phenolate para proton signal increased by roughly 4-fold, whereas the meta proton signal increased by more than 100-fold (Figure 2B). The increased line width of the phenolate para proton signal is likely due to greater hyperfine broadening at lower temperature caused by some temperature dependence of the electronic relaxation time.[43] Although complete decoalesence of the meta protons was not observed, the steep increase in the line width at low temperature is most reasonably explained by exchange broadening from slower rotation of the phenolate ring. Assuming a two-state model for this exchange broadening, the temperature-dependence can be fit with two adjustable parameters: the activation barrier, $\Delta G^{\ddagger}$, and the difference in the chemical shift of the two meta proton signals, $\Delta\delta$.[43] We accounted for the change in line width of the meta proton signal from hyperfine broadening by assuming it to be equal to that of the para proton signal. Since an estimation of the contact contribution (from the DFT calculation described below) and dipolar contribution to the paramagnetic relaxation

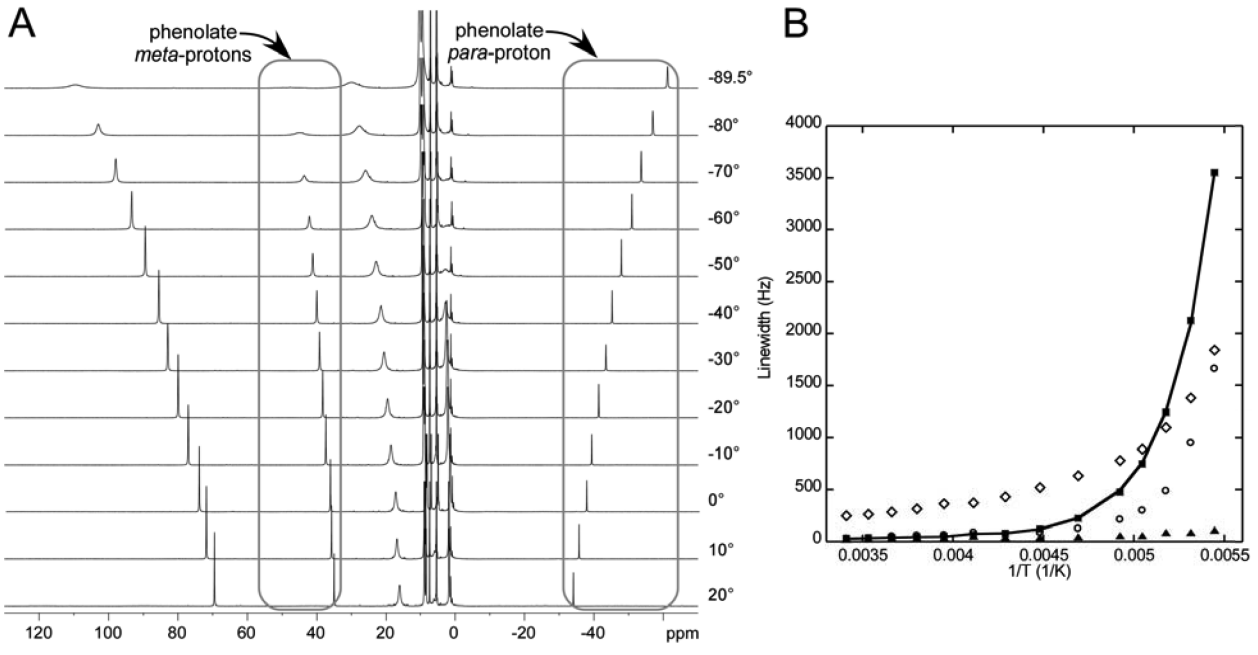

Figure 2. (A) Variable temperature ^{1}H NMR spectra of **3** in CD_2Cl_2. The phenolate meta and para protons are highlighted. (B) The temperature dependence of line width of the pyrazole H4 (○), phenolate meta (■), Tp-*ortho*-phenyl (◊), and phenolate para (▲) proton signals. The fit to the temperature dependence of the line width of the phenolate meta protons due to exchange broadening as described in the text is shown as a solid line.

dx.doi.org/10.1021/ic501424e | *Inorg. Chem.* 2014, 53, 9837−9848

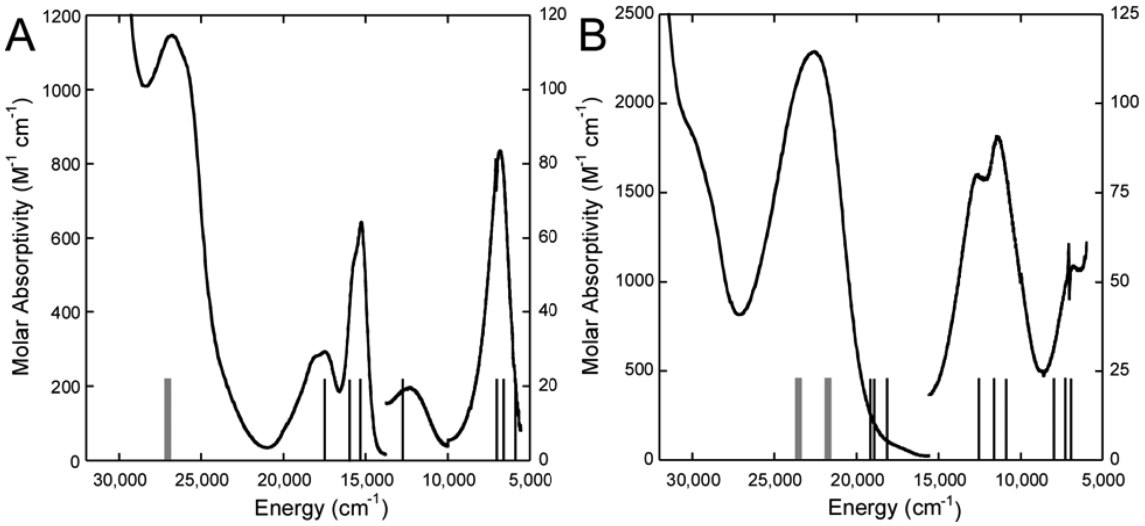

Figure 3. UV−vis−NIR absorption spectra of **3** (A) and **5** (B) in $CHCl_3$ at room temperature. The thin black bars indicate the calculated energies of the LF transitions from an AOM calculation, and the thick gray bars indicates the calculated energies of the phenolate oxygen pπ to metal CT transitions with high oscillator strengths from a TD-DFT calculation.

yields an average line width for the meta protons that is ∼1.8 that of the para proton, this assumption is justified. With these assumptions, the fit to the temperature dependence of the meta proton line width (Figure 2B, solid line) yielded $\Delta G^{\ddagger}$ = 30.3 ± 0.7 kJ/mol and $\Delta\delta$ = 3.4 ± 0.7 ppm. When the meta proton line width was fit assuming that exchange broadening was the sole contribution, the values of $\Delta G^{\ddagger}$ and $\Delta\delta$ were the same within uncertainty. The pyrazole H4 and *ortho*-phenyl proton signals of the Tp^{Ph2} ligand also showed evidence of exchange broadening at low temperature, but were not analyzed quantitatively.

Similar results were obtained using the VT-NMR spectra of **5** (Figure S2). Applying the same data analysis described above, the fit to the temperature dependence of the meta proton line width (Figure S2B, solid line) yielded $\Delta G^{\ddagger}$ = 37 ± 1 kJ/mol and $\Delta\delta$ = 0.7 ± 0.5 ppm. However, the reliability of these values is reduced compared with the results for complex **3** because of two factors. First, NMR spectra of this sample could only be obtained down to −70 °C. Second, the line width of the para proton signal increased with decreasing temperature to a greater extent (about 7-fold), presumably due to a larger temperature dependence to the hyperfine broadening. Since a larger proportion of the line width of the meta protons is also likely due to hyperfine broadening and not just exchange broadening, the calculated values of $\Delta G^{\ddagger}$ and $\Delta\delta$ will be much more sensitive to this correction. The assumption made here, that this paramagnetic contribution to the line broadening is the same for both the meta and para protons, may not be accurate, which in turn reduces the accuracy of the fitted values for $\Delta G^{\ddagger}$ and $\Delta\delta$.

Electronic Absorption Spectroscopic Studies. UV−vis−NIR absorption spectra were obtained for complexes **3**−**6** in $CHCl_3$. The spectra of **3** and **5** are given in Figure 3 (the spectra of **4** and **6** were nearly identical and are given in Figure S3). For **3**, prominent peaks were seen at 26800, 17480, 15270, 12330, and 6810 cm^{-1} (373, 572, 655, 811, and 1469 nm). The transition at 26800 cm^{-1} was the most intense (ε = 1150 M^{-1} cm^{-1}) and was assigned as a charge transfer (CT) transition from the phenolate-O pπ to the cobalt(II), analogous to the thiophenolate-S pπ to cobalt(II) CT transition reported previously for a closely related Tp^{iPr2}Co(penta-fluorothiophenolate) complex (28000 cm^{-1}, ε = 1300 M^{-1} cm^{-1}).[44] The other peaks were assigned as ligand field (LF) transitions of the cobalt(II). The absorption peaks for **5** appeared at 22600, 12700, 11400, and 6800 cm^{-1} (443, 788, 877, and 1470 nm). Likewise, the intense transition at 22600 cm^{-1} (ε = 2300 M^{-1} cm^{-1}) was assigned as a phenolate-O pπ to nickel(II) CT transition, analogous to the previously reported thiophenolate-S pπ to nickel(II) CT transition (23200 cm^{-1}, ε = 3060 M^{-1} cm^{-1}),[44] while the other peaks were assigned as LF transitions.

Mull absorption spectra of **3** and **5** were obtained in the UV−visible region, and the features of these spectra appeared at the same wavelengths as in the solution spectra. This indicates that the electronic structures of these complexes in solution are essentially the same as that in the solid state. This strongly argues that, while these complexes are fluxional in solution (as indicated by the ^{1}H NMR spectra), the geometric structure of the energy minimum in solution resembles the structure observed in the solid state. This, in turn, suggests that the metal−halogen secondary bond is present in the minimum energy solution structure.

The LF transitions of **3** were analyzed by the angular overlap method (AOM) using the AOMX program.[45] The AOM parameters of the analogous ($Tp^{t\text{-}Bu,R}$)CoL complexes (R = H, methyl, or 2′-thienyl; L = NCS^-, NCO^-, N_3^-, or Cl^-) of Krzystek et al.[46] were used as a starting point. The geometry from the crystal structure was used. The pyrazole nitrogens (N-pz) were treated as σ-donors and the phenolate oxygen (O-phen) was treated as a σ-donor and an out-of-plane π-donor.[47] An excellent fit was obtained with values of ε_σ(N-pz) = 4120, ε_σ(O-phen) = 2050, ε_π(O-phen) = 1660, and B = 698 cm^{-1} (C/B was kept fixed at 4.3). The calculated energies of the LF transitions are shown as thin black bars in Figure 3A. A C_s symmetrized structure of **3** was also used in an AOM analysis of the LF transitions. In this structure, the O1−Co−N_{eq}, N3−Co−N_{eq}, and Cl−Co−N_{eq} bond angles were averaged, and the phenolate was taken to be exactly coplanar with the N3−Co−O plane. Again, an excellent fit to the LF transitions could be obtained with very similar AOM parameters to those above (the only significant change was that ε_π(O-phen) increased to 1930 cm^{-1}). When the halogen was included as a σ-donor in the fit, optimization led to an unphysical (negative) value for

dx.doi.org/10.1021/ic501424e | *Inorg. Chem.* 2014, 53, 9837−9848

Table 3. Energies and Major Orbital Contributions of the β-Spin MOs with Predominantly Metal d and Phenolate O Orbital Character, from the PBE1PBE Calculations

	Tp*Co(2,6-dcp)			Tp*Ni(2,6-dcp)		
orbital	label	energy (eV)	contributions	label	energy (eV)	contributions
d_{z^2}	LUMO+2	−0.30	50% M, 2% N_{ax}, 9% N_{eq}, 2% Cl	LUMO+1	−1.08	81% M, 5% N_{ax}, 3% Cl
d_{xy}	LUMO+1	−0.53	56% M, 3% N_{ax}, 5% N_{eq}	LUMO	−1.30	80% M, 6% N_{eq}
$d_{x^2-y^2}$	LUMO	−1.23	86% M, 3% O, 5% N_{eq}	HOMO−10	−8.67	67% M, 7% O
phenolate-O pπ	HOMO	−5.75	7% M, 22% O, 60% phenyl C, 9% Cl	HOMO	−5.82	3% M, 23% O, 64% phenyl C, 9% Cl
d_{xz}	HOMO−1	−6.64	47% M, 3% O, 16% N_{eq}	HOMO−13	−9.22	62% M, 15% O, 4% Cl
d_{yz}	HOMO−4	−6.77	28% M, 12% N_{ax}, 5% N_{eq}, 3% Cl	HOMO−11	−8.78	47% M, 14% phenyl C, 26% Cl[a]
phenolate-O pσ	HOMO−8	−7.80	29% M, 14% O, 17% N_{eq}	HOMO−8	−7.39	28% M, 44% O, 3% N_{eq}
phenolate-O pσ	HOMO−10	−8.29	20% M, 44% O, 16% Cl			

[a]12% from proximal (coordinating) Cl, 14% from distal Cl.

ε_σ(Cl). Constraining ε_σ(Cl) to be positive led to an optimum fit with ε_σ(Cl) ≈ 0. If the ε_σ(N-pz) parameters were allowed to differ for the axial versus equatorial positions, then fits could be obtained with any combination of ε_σ(N_{ax}-pz) and ε_σ(Cl) such that the sum was ∼3100 cm^{-1}. Keeping the angular overlap parameters fixed while altering the angle ψ, which corresponds to rotation of the phenolate, altered the energies of the LF transitions by as much as 1700 cm^{-1}. These results suggest that (1) the phenolate remains approximately coplanar with the N3−Co−O plane in the minimum energy solution geometry, and (2) the metal−halogen secondary bond makes a negligible contribution to the LF splitting of the cobalt(II).

A similar analysis of the LF transitions of **5** was performed, using the AOM parameters of Tp*NiL (Tp* = tris(3,5-dimethylpyrazolyl)borate; L = Cl^-, Br^-, I^-) of Derochers et al.[48] as well as of complex **3** as a starting point. Since only three LF transitions could be clearly resolved (three more were assumed to be under the shoulder observed at 17000−19000 cm^{-1}), ε_π(O-phen) was constrained to be equal to 0.8 of ε_σ(O-phen). Again, using the geometry from the crystal structure, an excellent fit was obtained with ε_σ(N-pz) = 4660, ε_σ(O-phen) = 1830, ε_π(O-phen) = 1470, and B = 539 cm^{-1} (C/B was kept fixed at 4.7), and the calculated LF transition energies are shown in Figure 3B. As in the case of **3**, a C_s symmetrized structure of **5** was used, and again a reasonable fit to the LF transitions could be obtained with very similar AOM parameters. Likewise, inclusion of the metal−halogen secondary bond was not necessary to yield reasonable results for the energies of the LF transitions.

Density Functional Theory Calculations. Density functional theory calculations were performed on models of **3** and **5** with Gaussian[49] using both the B3LYP[50] and PBE1PBE[51] functionals. The phenyl groups of the Tp^{Ph2} ligand were replaced with methyl groups (Tp*). Geometry optimization with the 6-311++G(d) basis set for Cl and 6-311+G(d) basis set for all other atoms yielded excellent agreement with the experimentally determined structures with both functionals, with the exception of the metal−halogen distance (Table S1). Both DFT methods systematically calculated the metal−halogen distance to be longer than the experimentally determined values; however, M−X distances calculated with PBE1PBE for Tp*Co(2,6-dcp) and Tp*Ni(2,6-dcp) were 0.07 and 0.14 Å longer than the experimental values, respectively, while B3LYP gave values that were 0.20 and 0.29 Å longer. Constraining the metal-chlorine distance in Tp*Co(2,6-dcp) to the experimental value altered the total energy by only 1.5 kJ/mol in the B3LYP calculation. This is consistent with what has been previously postulated regarding metal−halogen bonding, namely, that the potential energy well is much shallower for a secondary bond than for a covalent bond, and thus the energy varies only slightly as the distance changes.[16]

The ground state electronic structures of Tp*Co(2,6-dcp) and Tp*Ni(2,6-dcp) are typical for high-spin cobalt(II) and nickel(II) complexes, and strongly resemble the previously reported pentafluorothio-phenolate complexes.[44] There are three unoccupied β-spin orbitals in the Co(II) complex (d_{z^2}, d_{xy}, and $d_{x^2-y^2}$, defining the z and x axes to be approximately along the M−N_{ax} and M−O bond vectors, respectively) and two in the Ni(II) complex (d_{z^2} and d_{xy}). In both cases, the β-spin HOMO is the phenolate-O pπ orbital. Phenolate-O pσ orbital character was found distributed in two closely spaced β-spin MOs at much lower energies in Tp*Co(2,6-dcp) and in one in Tp*Ni(2,6-dcp). The energies and major orbital contributions, determined from the Mulliken orbital contributions[52−55] from the PBE1PBE calculations with a smaller basis set (6-311G(d)) analyzed with AOMix,[56,57] are given in Table 3, and contour surface plots of the orbitals of Tp*Co(2,6-dcp) are shown in Figure S4 (very similar results were obtained with B3LYP). Small Cl contributions are seen in two of the β-spin d orbitals in both complexes: d_{z^2} has a small σ interaction, and d_{yz} has a small π interaction. In Tp*Ni(2,6-dcp), d_{xz} also shows some interaction with the Cl.

Mayer bond orders[58−61] were calculated in order to quantify the extent of the metal−halogen interaction. Since calculations with the large, diffuse basis set used for the geometry optimization gave unphysical values for the bond orders, single-point calculations with the 6-311G(d) basis set were used. These results yielded a M−Cl bond order that is about 15−38% of the bond orders for the M−O and M−N bonds (Table 4). Similar results were obtained from the Wiberg and Löwdin bond indices (Table S2).[62] Thus, the calculations show that while the chlorine has some bonding interaction with the metal, it is considerably smaller than that of the "normal" metal−ligand bonds.

In order to obtain a quantitative estimate of the strength of the metal-chlorine interaction, the barrier to rotation of the

Table 4. Mayer Bond Orders for Tp*M(2,6-dcp)

bond	M = Co	M = Ni
M−O	0.398	0.351
M−$N3_{(ax)}$	0.244	0.271
M−$N1_{(eq)}$	0.255	0.265
M−$N5_{(eq)}$	0.255	0.287
M−Cl	0.059	0.100

dx.doi.org/10.1021/ic501424e | Inorg. Chem. 2014, 53, 9837−9848

phenolate about the O−C bond was examined in Tp*Co(2,6-dcp). For Tp*Co(2,6-dcp), the Co−O1−C46$_{phen}$-C47$_{phen}$ torsion angle in the optimized geometry was 0°. This angle was then was fixed at 15°, and the geometry was reoptimized. This was repeated at 15° increments up to 90°. From this, the calculated barrier to rotation of the phenolate was found to be 10.3 kJ/mol with B3LYP and 13.4 kJ/mol with PBE1PBE (Figure 4 and Table S3). Likewise for Tp*Ni(2,6-dcp), the

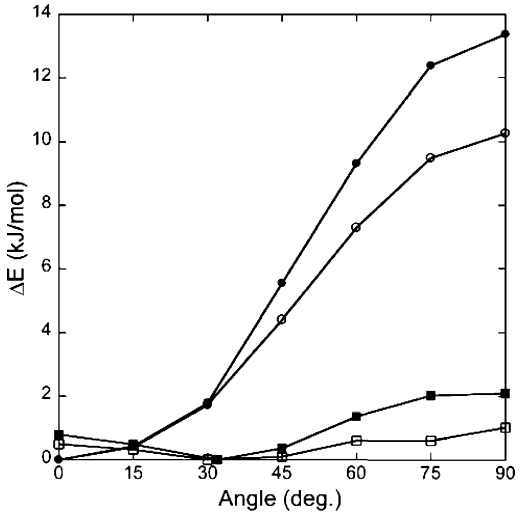

Figure 4. Barrier to rotation of the phenolate in Tp*Co(2,6-dichlorophenolate) (circles) and Tp*Co(2,6-dimethylphenolate) (squares), calculated with B3YLP (open symbols) and PBE1PBE (filled symbols). The Co−O1−C46$_{phen}$−C47$_{phen}$ torsion angle was fixed at 15° increments from 0° to 90° and the geometry was reoptimized.

energy difference with PBE1PBE between the fully optimized geometry, where the Ni−O1−C46$_{phen}$-C47$_{phen}$ torsion angle was −4.8°, and one in which the torsion angle was frozen at 105° was found to be 9.7 kJ/mol (the torsion angle of 90° created a steric clash with the methyl group of the Tp* ligand and had difficulty converging).

Two alternative factors must be considered that could contribute to a barrier to rotation of the phenolate ring besides the metal−halogen secondary bond. The first is steric hindrance from the phenyl substituents of the Tp^{Ph2} ligand. Because the size of the substituents on the Tp ligand was reduced from phenyl to methyl in the DFT calculation, this should have reduced the effect of any steric hindrance on rotation of the phenolate in the calculations. Additionally, we note that when the Co−O1−C46$_{phen}$−C47$_{phen}$ dihedral angle in **3** was frozen at 90°, the steric clash between the chloro substituent and the phenyl ring of the Tp^{Ph2} ligand could be readily relieved by rotation of the phenyl ring. This suggests that while there may be greater steric hindrance from the Tp^{Ph2}, it is probably not severe.

The second factor is the anisotropic π-bonding of the phenolate-O to the metal center. To address how this might influence the energy barrier to rotation of the phenolate, calculations were performed on a complex in which the 2,6-dcp ligand was replaced with 2,6-dimethylphenolate (2,6-dmp), with the Co−O1−C46$_{phen}$−C47$_{phen}$ torsion angle again stepped in 15° increments from 0° to 90°. This yielded an extremely low barrier to rotation (Figure 4, Table S4), indicating that π-bonding of the phenolate-O does not contribute to the energetics of phenolate rotation.

While the actual mode of geometric fluxionality of these complexes in solution is likely more complex, the calculated low barrier to rotation of the phenolate is qualitatively consistent with the low barrier to rotation that was determined experimentally from VT-NMR. However, the DFT calculation underestimated this barrier by a factor of ∼2.3 for the cobalt(II) and by even more for the nickel(II) complex. The lack of quantitative agreement could be due to two factors: (1) additional steric hindrance from the phenyl substituents on the Tp ligand could raise this barrier in the actual complex (as noted above) and (2) DFT methods, while highly successful at describing open-shell transition metal complexes, are often poor at accurately calculating weak noncovalent interactions.[63] While the PBE1PBE functional performed better than B3LYP with regards to both the metal−halogen distance and the barrier to rotation, in agreement with previous claims regarding the utility of these functionals for the calculation of noncovalent interactions,[63] the energy difference in the latter was small. Note that the best density functional for noncovalent interactions, M06X, failed to give a reasonable electronic structure description for the metal. Nonetheless, the fact that DFT calculations yield a barrier to rotation for Tp*Co(2,6-dcp) but not for Tp*Co(2,6-dmp) provides the strongest evidence that the experimentally observed barrier comes mainly from the metal−halogen interaction and not steric hindrance or anisotropic π-bonding of the phenolate.

Time-dependent DFT (TD-DFT), calculated with B3LYP using the PBE1PBE-optimized structure, was used to calculate the energies of the phenolate-O to metal CT transitions in the cobalt(II) and nickel(II) 2,6-dcp complexes. In the fully geometry-optimized Tp*Co(2,6-dcp), three phenolate O pπ to cobalt(II) CT transitions are observed: pπ → $d_{x^2-y^2}$ (22600 cm^{-1}), pπ → d_{xy} (27100 cm^{-1}), and pπ → d_{z^2} (30300 cm^{-1}). Only the pπ → d_{xy} has an oscillator strength >0.0005 (f = 0.0296), in excellent agreement with the experimentally observed intense transition at 26800 cm^{-1} in the solution spectrum. In the TD-DFT calculation of Tp*Co(2,6-dcp) with the Co−O1−C46$_{phen}$−C47$_{phen}$ torsion angle frozen at 90°, the three pπ CT transitions occur at very similar energies: pπ → $d_{x^2-y^2}$ (22200 cm^{-1}), pπ → d_{xy} (27700 cm^{-1}), and pπ → d_{z^2} (28000 cm^{-1}); however, the oscillator strength of the pπ → d_{xy} transition has dropped to 0.0001 while that of the lower energy pπ → $d_{x^2-y^2}$ transition has increased to 0.0444. Similar results are obtained with the TD-DFT calculation of Tp*Ni(2,6-dcp). Two closely spaced phenolate-O pπ to nickel(II) CT transitions are observed, pπ → d_{xy} (21700 cm^{-1}) and pπ → d_{z^2} (23500 cm^{-1}), with similar oscillator strengths (f = 0.0501 and 0.0216, respectively). This again agrees well with the experimentally observed intense transition at 22600 cm^{-1} in the solution spectrum.

Overall, the results indicate that the minimum energy solution geometry in each complex is one in which the torsion angle of the phenolate is ∼0°, since this geometry is the one predicted to give an intense CT transition at the energy where it is observed in the solution absorption spectrum. This, in turn, agrees with crystal structures and with the mull UV−visible absorption spectra. So, while complexes **3** and **5** are fluxional in solution, there is a discrete energy minimum in the geometry.

dx.doi.org/10.1021/ic501424e | Inorg. Chem. 2014, 53, 9837−9848

Table 5. Comparison of M−X Distances for Complexes 1−6 and Other Iron(II), Cobalt(II), and Nickel(II) *ortho*-Halophenolate Complexes, the Average Metal−Halide Bond Lengths, and the Difference (Δ M−X)

	complex[a]	experimental M−X distance (Å)[b]	average bond length (Å)[c]	ΔM−X (Å)	ref
Fe−Cl	**1**	2.862	2.301	0.561	
	(TACH-*o*-tolyl)Fe(2,6-dcp)	2.890−3.122	2.301	0.589−0.821	15
	(TACH-*o*-tolyl)Fe(2-cp)	2.929, 3.010	2.301	0.628, 0.709	15
Fe−Br	**2**	2.885	2.35	0.54	
	(TACH-*o*-tolyl)Fe(2,6-dbp)	2.841	2.35	0.49	15
Co−Cl	**3**	2.833	2.254	0.579	
	$Co(NMIm)_2(2,4,6\text{-tcp})_2$	3.100	2.254	0.846[d]	22
	$[Co(OMe)(2,4,6\text{-tcp})(MeOH)]_4$	2.62, 2.64	2.414[e]	0.21, 0.23[d]	24
	$Co(TMED)(2,4,6\text{-tcp})_2$	2.873, 2.894	2.414[e]	0.459, 0.480	25
Co−Br	**4**	2.811	2.384	0.427	
	$Co(py)_2(2,4,6\text{-tbp})_2$	3.116, 3.120	2.573[e,f]	0.543, 0.547	27
	$Co(NMIm)_2(2,4,6\text{-tbp})_2$	3.027, 3.091	2.573[e,f]	0.454, 0.518	26
Ni−Cl	**5**	2.560	2.217	0.343	
	$[Ni(OMe)(2,4,6\text{-tcp})(MeOH)]_4$	2.483−2.530	2.441[e]	0.042−0.089[d]	23
	$Ni(TMED)(2,4,6\text{-tcp})_2$	2.586, 2.637	2.441[e]	0.145, 0.196[d]	19
Ni−Br	**6**	2.685	2.341	0.344	

[a]Other abbreviations: 2-chlorophenolate (2-cp), *N*-methylimidazole (NMIm), 2,4,6-trichlorophenolate (2,4,6-tcp), *N,N,N′,N′*-tetramethyl-1,2-ethanediamine (TMED), pyridine (py), 2,4,6-tribromophenolate (2,4,6-tbp). [b]Different M−X distances are either due to multiple coordinated *ortho*-halophenolates, or from different crystal forms and/or multiple conformers in the same unit cell. [c]For four-coordinate divalent metal complexes, unless otherwise noted. [d]NQR results indicate the presence of a metal−halogen secondary bond.[17,19] [e]For six-coordinate complexes. [f]This value was not available in ref 21; therefore, it was determined from 31 structures in the Cambridge Structural Database of six-coordinate cobalt complexes with one or more terminal bromide ligands where the oxidation state was unambiguously Co(II).

DISCUSSION

The model complexes reported here serve to further illuminate the nature of the metal−halogen secondary bonding observed with *ortho*-dihalophenolates, and thus the potential binding modes of substrates and inhibitors at the active site of PcpA.[14] To our knowledge, this is the only case where metal−halogen bonding has been reported for a series of structurally homologous complexes where the identity of both the metal and the halogen is varied. Thus, these complexes can provide valuable insights into the nature and influence of this interaction. We use a combination of crystallography, NMR spectroscopy, and spectroscopically calibrated computational methods to quantify and elucidate this important interaction.

In the crystal structures of complexes **1**−**6**, the halogen occupies an axial position of a distorted trigonal bipyramidal geometry. According to the criterion established by Wulfsberg, a metal−halogen secondary bond is present if the metal−halogen distance is less than the average metal-halide distance plus 1 Å.[19] By this definition, all six of these complexes exhibit metal−halogen secondary bonding. The metal−halogen distances of these complexes as well as those of other iron(II), cobalt(II), and nickel(II) *ortho*-halophenolate complexes exhibiting metal−halogen secondary bonding are reported in Table 5, along with the average metal-halide bond lengths for divalent metal complexes,[21] and the difference between these (ΔM-X). The previously reported Co(*N*-methylimidazole)$_2$(2,4,6-trichlorophenolate)$_2$ complex is a particularly useful comparison, since it is also five-coordinate (τ = 0.43) when counting the chlorine.[22] The trend in metal−halogen distance among complexes **1**−**6** is Fe > Co > Ni, which is in accordance with the trend in ionic radii of these divalent metal ions, as well as the expected increase in Z_{eff}. The metal−halogen distances are particularly short in the nickel(II) complexes, although within the range of the remarkably short distances seen in some other nickel(II)-*ortho*-chlorophenolate complexes (2.483−2.530[23] and 2.586 Å[19]). However, these complexes were six-coordinate when including the secondary bonds, so using a six-coordinate average Ni−Cl (2.441 Å), ΔM−X was much smaller.

The Tp complexes reported here exhibit no clear trend in metal−halogen distance or in ΔM−X between the 2,6-dichloro- and 2,6-dibromophenolates. Since the van der Waals radius of bromine is larger than that of chlorine,[40,41] one might predict that the metal−bromine distances would be longer than the corresponding metal-chlorine distances. Conversely, if the secondary bonding interaction were stronger for the more polarizable halogen,[64] one might predict the opposite trend. However, the strength of secondary bonding has been postulated to be only weakly dependent on distance,[16] and the results of our DFT calculations on these complexes suggest only weak covalent bonding between the metal and the halogen. Thus, the very shallow potential energy well for this interaction may make it too difficult to discern a trend in M−Cl versus M−Br distances even in these structurally related complexes.

These Tp-supported complexes are all fluxional on the NMR time scale. Therefore, one must consider whether the metal−halogen secondary bond observed in the crystal structures is also present in solution. A comparison of the mull and solution spectra show that the transitions in the UV−visible region are at the same energies, arguing that the geometry is the same in both the solid and the minimum energy solution state structures. Likewise, the TD-DFT calculation of the energy of the intense phenolate-O to metal CT transition is only consistent with a structure where the Co−O1−C46$_{phen}$−C47$_{phen}$ torsion angle is ∼0°. Therefore, we conclude that the secondary bond is not an artifact of crystallization and is present in the minimum energy solution structure.

The ultimate question is whether the halogen is truly a "ligand." A simple AOM analysis of the LF transitions in the UV−vis-NIR absorption spectra was entirely consistent with a trigonal pyramidal geometry, without including the halogen.

dx.doi.org/10.1021/ic501424e | Inorg. Chem. 2014, 53, 9837−9848

Although the DFT calculations do show a small percentage of chlorine character mixed into the metal d-orbitals, calculations give a bond order that is only 15−38% of the values for the M−O and M−N bonds. From VT-NMR, the experimentally determined value for the phenolate barrier to rotation was 30.3 kJ/mol in **3** and 37 kJ/mol in **5** (with the caveat noted above). The DFT calculations with PBE1PBE gave a barrier to rotation of the phenolate in Tp*Co(2,6-dcp) of just 13.4 kJ/mol, and the barrier in the nickel(II) complex was comparable. The evidence herein suggests that the metal−halogen interaction in these compounds is primarily electrostatic in nature and that there is no significant covalent interaction between the metal and halogen.

For comparison, another type of noncovalent interaction involving polarizable halogens (especially attached to arenes) is halogen bonding, where a halogen interacts with the partial negative charge on an oxygen or nitrogen atom[42,65,66] or with the π electrons from an aromatic ring.[67,68] The strength of this interaction has been estimated as 10−30 kJ/mol for haloarenes, which is similar to that for a hydrogen bond between neutral species.[69] Assuming that the barrier to rotation of the phenolate is a reasonable measure of the strength of the metal−halogen secondary bond, it puts the strength of the metal−halogen secondary interaction in the same range as halogen bonding. Note that the directionality of these two types of noncovalent interactions is very different, due to the strongly anisotropic charge distribution of polarizable halogens, in which electron density is pulled away from the crown of the halogen and drawn toward the equator.[42] Thus, while the ideal C-X···O/N angle in halogen bonding is ∼180°, the ideal C-X···M angle in metal−halogen secondary bonding is ∼90°, as observed in the present complexes.

These results further illuminate to what extent metal−halogen bonding could be responsible for the unusual specificity of the enzyme PcpA for *ortho*-dihalophenols and hydroquinones. Since this interaction gives a stabilization that is on par with other noncovalent interactions that govern binding of substrates and inhibitors to the active site pocket, metal−halogen secondary bonding is but one of several factors that must be considered in governing the substrate specificity of this enzyme, and further work is required to elucidate its potential role. Nonetheless, if one makes the rough assumption that in PcpA the K_{mA} is primarily determined by substrate binding ($\sim K_D$), then $\Delta\Delta G$ for binding of dihalohydroquinone versus dimethylhydroquinone is 7−9 kJ/mol, and thus secondary bonding could certainly be a large contributor to this difference. Metal−halogen secondary bonding could also play an important role in other ways; for example, it could help to orient the *ortho*-dihalohydroquinone substrates in a geometry that is optimal for attack by O_2, thus leading to the higher k_{cat} that is observed with *ortho*-dihalohydroquinone substrates relative to the *ortho*-dimethyl version.

EXPERIMENTAL SECTION

General Considerations. All reagents were reagent grade and used without purification except where indicated. For the reactions with iron(II), the phenols were purified by sublimation before use, and THF was dried by distillation from sodium and benzophenone. For reactions with cobalt(II) and nickel(II), reagent grade anhydrous THF was used without further purification and CH_2Cl_2 was dried over molecular sieves. THF-d_8 was dried over CaH_2, then over sodium metal, and then vacuum distilled into a storage container before use. The tris(3,5-diphenylpyrazolyl)borate ligand, KTp^{Ph2}, was prepared by literature procedures.[31] All manipulations were carried out under an N_2 atmosphere using standard Schlenk techniques or in a glovebox maintained at or below 1.0 ppm of O_2, except crystallization of the cobalt(II) and nickel(II) complexes.

Spectra and Data Analysis. NMR spectra were collected on a Bruker Avance III 400 MHz spectrometer with a broadband probe. Variable temperature NMR spectra were acquired with an inverse broadband probe, and a liquid nitrogen heat exchanger was used to control the temperature. The temperature sensor in the probe was calibrated with neat methanol.[70] All peaks in NMR spectra of the complexes appeared as singlets and are reported in ppm. The temperature dependences of the linewidths in the variable temperature NMR spectra were fit in Excel (Microsoft) using Solver. The uncertainty in $\Delta G^{\ddagger}$ and $\Delta\delta$ was estimated with a jackknife procedure.[71] FT-IR measurements were carried out on KBr pellets and acquired on an PerkinElmer Avatar 360 or a Shimadzu Prestige 21 spectrometer. UV−visible absorption spectra were acquired on a Cary 50 Bio UV−visible spectrophotometer, and NIR absorption spectra were acquired on a StellarNet InGaAs spectrophotometer. Solution spectra were acquired in quartz cuvettes of 1 cm optical path length, while mull spectra were acquired in quartz cuvettes of 0.2 mm path length. Elemental analyses were determined by the CENTC Elemental Analysis Facility at the University of Rochester. X-ray crystallography was performed at the X-ray Crystallographic Facility of the Department of Chemistry at the University of Rochester.

Tp^{Ph2}MX. Tp^{Ph2}CoCl and Tp^{Ph2}NiBr were prepared according to literature methods.[37,38] Tp^{Ph2}FeBr was prepared in a similar manner to Tp^{iPr2}FeCl and characterized by ^{1}H NMR spectroscopy (Figure S5).[32]

Sodium 2,6-Dibromophenolate. To a solution of 2,6-dibromophenol (120.5 mg, 0.4784 mmol) in THF (4 mL), excess sodium hydride was added slowly until bubbling ceased. The solution was filtered through Celite. Solvent was removed under vacuum and a white powder was collected. Crystallization of the solid from THF (3 mL) gave clear, colorless crystals (0.0968 g, 73%). ^{1}H NMR (400 MHz, 25 °C, CD_3CN): δ 7.29 (d, 2, *meta*-H, J = 7.6 Hz), 6.03 (t, 1, *para*-H, J = 7.8 Hz) ppm.

Sodium 2,6-Dichlorophenolate. This was prepared by the method above using 2,6-dichlorophenol (146.7 mg, 0.9000 mmol). Crystallization yielded clear, colorless crystals (45.1 mg, 27% yield). ^{1}H NMR (400 MHz, 25 °C, CD_3CN): δ 7.12 (d, 2, *meta*-H, J = 8.0 Hz), 6.23 (t, 1, *para*-H, J = 7.8 Hz) ppm.

Tp^{Ph2}Fe(2,6-Dichlorophenolate) (1). Tp^{Ph2}FeBr (56.3 mg, 0.0699 mmol) was dissolved in THF (15 mL). The solution was transferred to solid sodium 2,6-dichlorophenolate (14.8 mg, 0.0800 mmol), and was stirred overnight. The solvent was removed under reduced pressure, and the product was suspended in acetonitrile (5 mL). The suspension was filtered through a Celite plug and washed with additional THF (5 mL). The THF was then removed, leaving an off-white powder. The product was redissolved in THF (2 mL) and crystallized via vapor diffusion with pentane to give colorless crystals (44.1 mg, 71% yield).[72] ^{1}H NMR (400 MHz, 25 °C, THF-d_8): δ 57.9 (3H, pz-H4), 54.2 (2H, *m*-phenolate), 39.2 (1H, BH), 16.4 (6H, *o/m*-Ph), 12.8 (6H, *o/m*-Ph), 10.0 (3H, *p*-Ph), 7.0 (∼10H, *o/m/p*-Ph), −21.8 (∼4H, *o/m/p*-Ph), −23.7 (1H, *p*-phenolate) ppm. IR (KBr): 3061 (w), 2634 (w), 1575 (s), 1544 (s), 1479 (m), 1456 (w), 1415 (m), 1301 (w), 1168 (w), 1066 (w), 759 (w), 696 (s) cm^{-1}. Elem. Anal.: Calculated for $C_{51}H_{37}BCl_2FeN_6O$•THF: C, 68.84; H, 4.73; N, 8.76. Found: C, 69.02; H, 4.85; N, 8.79.

Tp^{Ph2}Fe(2,6-Dibromophenolate) (2). This was prepared as for **1**, but using Tp^{Ph2}FeBr (50.5 mg, 0.0627 mmol) and sodium 2,6-dibromophenolate (19.0 mg, 0.0694 mmol). Crystallization via vapor diffusion with pentane to give colorless crystals (46.8 mg, 76% yield). ^{1}H NMR (400 MHz, 25 °C, THF-d_8): δ 58.4 (3H, pz-H4), 54.3 (2H, *m*-phenolate), 35.7 (1H, BH), 15.5 (6H, *o/m*-Ph), 12.4 (6H, *o/m*-Ph), 9.6 (3H, *p*-Ph), 6.7 (∼9H, *o/m/p*-Ph), −19.22 (∼4H, *o/m/p*-Ph), −26.18 (1H, *p*-phenolate) ppm. IR (KBr): 3061 (w), 2625 (w), 1564 (s), 1544 (s), 1479 (s), 1452 (m), 1415 (s), 1305 (m), 1168 (w), 1066 (w), 763 (m), 696 (s) cm^{-1}. UV−vis−NIR (in THF) λ_{max} (ε/M^{-1} cm^{-1}) 360 (sh) nm. Elem. Anal.: Calculated for $C_{51}H_{37}BBr_2FeN_6O$•THF: C, 63.01; H, 4.33; N, 8.02. Found: C, 62.76; H, 4.26; N, 7.95.

dx.doi.org/10.1021/ic501424e | Inorg. Chem. 2014, 53, 9837−9848

Table 6. Crystal and Data Parameters for Structures 1−6

	1	2	3	4	5	6
empirical formula	$C_{51}H_{37}BCl_2FeN_6O$	$C_{53}H_{41}BBr_2FeN_6O_{1.5}$	$C_{51}H_{37}BCl_2CoN_6O$	$C_{51}H_{37}BBr_2CoN_6O$	$C_{51}H_{37}BCl_2NiN_6O$	$C_{51}H_{37}Br_2NiN_6O$
formula weight	887.43	1012.40	890.51	979.43	890.29	979.21
temperature (K)	100.0(5)	100.0(5)	100.0(5)	100.0(5)	100.0(5)	100.0(5)
wavelength (Å)	0.71073	0.71073	0.71073	0.71073	0.71073	0.71073
crystal system	triclinic	triclinic	monoclinic	monoclinic	triclinic	triclinic
space group	*P*-1	*P*-1	$P2_1/n$	$P2_1/n$	*P*-1	*P*-1
a (Å)	12.305(2)	12.4836(11)	10.2718(15)	10.2332(11)	12.3898(11)	12.4504(15)
b (Å)	14.638(3)	12.8222(11)	30.796(4)	30.514(3)	14.2664(13)	12.8726(16)
c (Å)	15.082(3)	15.9833(14)	13.4527(19)	13.6761(15)	15.4042(13)	15.8829(19)
α (deg)	64.193(3)	89.687(2)	90	90	63.969(2)	90.729(2)
β (deg)	84.138(4)	79.109(2)	91.876(3)	91.362(2)	84.152(2)	100.184(2)
γ (deg)	71.675(4)	62.179(2)	90	90	71.450(2)	117.451(2)°
volume (Å^3)	2319.8(7)	2211.8(3)	4253.2(10)	4269.2(8)	2317.2(4)	2210.4(5)
Z	2	2	4	4	2	2
crystal color, morphology	colorless, block	colorless, needle	blue-violet, plate	blue-violet, plate	yellow-orange, block	yellow-orange, plate
crystal size (mm)	0.24 × 0.20 × 0.08	0.22 × 0.18 × 0.12	0.24 × 0.18 × 0.06	0.22 × 0.18 × 0.05	0.20 × 0.20 × 0.16	0.18 × 0.14 × 0.05
data/restraints/parameters	18368/0/559	16767/5/592	8696/0/559	7550/0/559	17565/0/559	7809/0/559
GOF on F^2	0.873	0.998	1.086	1.035	0.909	0.870
final *R* indices [$I > 2\sigma(I)$]	*R*1 = 0.0563, *w*R2 = 0.1170	*R*1 = 0.0535, *w*R2 = 0.1021	*R*1 = 0.0662, *w*R2 = 0.1163	*R*1 = 0.0594, *w*R2 = 0.1015	*R*1 = 0.0582, *w*R2 = 0.1138	*R*1 = 0.0634, *w*R2 = 0.1057
R indices (all data)	*R*1 = 0.1107, *w*R2 = 0.1356	*R*1 = 0.1159, *w*R2 = 0.1224	*R*1 = 0.1150, *w*R2 = 0.1322	*R*1 = 0.1189, *w*R2 = 0.1181	*R*1 = 0.0970, *w*R2 = 0.1292	*R*1 = 0.1447, *w*R2 = 0.1276

Tp^{Ph2}Co(2,6-Dichlorophenolate) (3). A solution of Tp^{Ph2}CoCl (15 mg, 0.020 mmol) in THF (4 mL) was added to sodium 2,6-dichlorophenolate (80 mg, 0.043 mmol). Upon addition, the solution changed from aqua blue to purple. The reaction was stirred for 3 h, the solution was filtered, and solvent was removed under reduced pressure. Crystallization from CH_2Cl_2 (2 mL) layered with hexanes (8 mL) yielded purple crystals (12 mg, 74%). ^{1}H NMR (400 MHz, 25 °C, $CDCl_3$): δ 68.1 (3H, pz-H4), 35.2 (2H, *m*-phenolate), 15.1 (6H, *o*-Ph), 9.08 (6H, *o*/*m*-Ph), 8.85 (6H, *o*/*m*-Ph), 8.67 (3H, *p*-Ph), 8.196 (6H, *o*/*m*-Ph), 7.45 (3H, *p*-Ph), −34.1 (1H, *p*-phenolate) ppm. IR (KBr): 3123 (w), 2626 (w), 1546 (m), 1475 (s), 1169 (s), 760 (s), 695 (s) cm^{-1}. UV−vis−NIR (in $CHCl_3$) λ_{max} (ε/M^{-1} cm^{-1}) 373 (1190), 572 (283), 655 (620), 811 (19), 1469 (81) nm. Elem. Anal. Calculated for $C_{51}H_{37}BCl_2CoN_6O$: C, 68.78; H, 4.19; N, 9.44. Found: C, 68.31; H, 4.18; N, 9.38.

Tp^{Ph2}Co(2,6-Dibromophenolate) (4). This was prepared as for **3**, but using Tp^{Ph2}CoCl (12 mg, 0.016 mmol) and sodium 2,6-dibromophenolate (6.0 mg, 0.022 mmol). Crystallization from CH_2Cl_2 (2 mL) layered with hexanes (10 mL) yielded purple crystals (13 mg, 80%). ^{1}H NMR (400 MHz, 25 °C, $CDCl_3$): δ 67.4 (3H, pz-H4), 37.3 (2H, *m*-phenolate), 10.5 (6H, *o*-Ph), 9.90 (6H, *o*/*m*-Ph), 8.92 (6H, *o*/*m*-Ph), 8.30 (3H, *p*-Ph), 7.78 (9H, *o*/*m*/*p*-Ph), −34.7 (1H, *p*-phenolate) ppm. IR (KBr): 3129 (m), 2620 (w), 1451 (s), 1168 (s), 760 (s), 697 (s) cm^{-1}. UV−vis−NIR (in $CHCl_3$) λ_{max} (ε/M^{-1} cm^{-1}) 372 (1230), 570 (273), 660 (539), ∼800 (∼20), 1475 (71) nm. Elem. Anal. Calculated for $C_{51}H_{37}BBr_2CoN_6O$: C, 62.54; H, 3.81; N, 8.58. Found: C, 62.88; H, 3.90; N, 8.53.

Tp^{Ph2}Ni(2,6-Dichlorophenolate) (5). This was prepared as for **3**, but using Tp^{Ph2}NiBr (19 mg, 0.024 mmol) and sodium 2,6-dichlorophenolate (5.4 mg, 0.029 mmol). Crystallization from CH_2Cl_2 (3 mL) layered with hexanes (5 mL) yielded orange crystals (12 mg, 58%). ^{1}H NMR (400 MHz, 25 °C, $CDCl_3$): δ 72.4 (3H, pz-H4), 29.0 (2H, *m*-phenolate), 11.5 (6H, *o*-Ph), 8.52 (3H, *p*-Ph), 7.20 (9H, *o*/*m*/*p*-Ph), 6.73 (6H, *o*/*m*-Ph), 6.63 (6H, *o*/*m*-Ph), −16.8 (1H, BH), −25.2 (1H, *p*-phenolate) ppm. IR (KBr): 3060 (w), 2640 (w), 1653 (m), 1459 (s), 1174 (s), 1012 (s), 694 (s) cm^{-1}. UV−vis−NIR (in $CHCl_3$) λ_{max} (ε/M^{-1} cm^{-1}) 443 (2300), 788 (80), 877 (91), 1470 (53) nm. Elem. Anal. Calculated for $C_{51}H_{37}BCl_2NiN_6O\bullet$ 1/2CH_2Cl_2: C, 66.31; H, 4.11; N, 9.01. Found: C, 66.20; H, 4.56; N, 8.61.

Tp^{Ph2}Ni(2,6-Dibromophenolate) (6). This was prepared as for **3**, but using Tp^{Ph2}NiBr (13 mg, 0.016 mmol) and sodium 2,6-dibromophenolate (5.1 mg, 0.019 mmol). Crystallization from CH_2Cl_2 (2 mL) layered with hexanes (5 mL) yielded orange crystals (15 mg, 71%). ^{1}H NMR (400 MHz, 25 °C, $CDCl_3$): δ 71.3 (3H pz-H4), 28.0 (2H, *m*-phenolate), 10.4 (6H, *o*-Ph), 8.38 (3H, *p*-Ph), 6.78 (6H, *o*/*m*-Ph), 6.67 (6H, *o*/*m*-Ph), −16.1 (1H, BH), −25.3 (1H, *p*-phenolate) ppm. IR (KBr): 3131 (m), 2619 (w), 1546 (w), 1455 (s), 1173 (s), 760 (s), 696 (s) cm^{-1}. UV−vis−NIR (in $CHCl_3$) λ_{max} (ε/M^{-1} cm^{-1}) 447 (1790), 789 (55), 880 (63), ∼1500 (46) nm. Elem. Anal. Calculated for $C_{51}H_{37}BBr_2NiN_6O$: C, 62.56; H, 3.81; N, 8.58. Found: C, 62.29; H, 3.85; N, 8.50.

X-ray Crystallography. Each crystal was placed onto the tip of a glass fiber and mounted on a Bruker SMART Platform diffractometer equipped with an APEX II CCD area detector. All data were collected at 100.0(5) K using Mo Kα radiation (graphite monochromator). For each sample a preliminary set of cell constants and an orientation matrix were determined from reflections harvested from three orthogonal wedges of reciprocal space. Full data collections were carried out with frame exposure times of 45−120 s at detector distances of 4 cm. Randomly oriented regions of reciprocal space were surveyed for each sample: four or five major sections of frames were collected with 0.50° steps in ω at different φ settings and detector positions of −38° in 2θ. The intensity data were corrected for absorption,[73] and final cell constants were calculated from the xyz centroids of 3790−4087 (1804 in the case of **6**) strong reflections from the actual data collection after integration.[74] Structures were solved using SIR97[75] and refined using SHELXL-97.[76] Direct-methods solutions were calculated which provided most non-hydrogen atoms from the difference Fourier map. Least squares (on F^2) difference Fourier cycles located the remaining non-hydrogen atoms. Non-hydrogen atoms were refined with anisotropic displacement parameters and hydrogen atoms were placed in ideal positions and refined as riding atoms with relative isotropic displacement parameters. Details of each structure are given in Table 6.

Structures **1**, **5**, and **6** (**1** and **5** are isomorphous) were found to have cocrystallized solvent that was highly disordered and unable to be modeled satisfactorily. Reflection contributions from the solvent were removed using the SQUEEZE routine of program Platon,[77] which determined there to be 87, 115, and 59 electrons in 353, 375, and 169

dx.doi.org/10.1021/ic501424e | Inorg. Chem. 2014, 53, 9837−9848

Å^3 removed, respectively, per unit cell. Because the exact identity and amount of solvent were not known, no solvent was included in the atom list nor the molecular formulas for these structures; thus all calculated quantities that derive from the molecular formulas (i.e., F(000), density, molecular weight, etc.) are known to be incorrect. The asymmetric unit of structure **2** contained the iron molecule in a general position and one cocrystallized THF solvent molecule in a crystallographic inversion center, the latter which was modeled as disordered over the center. Structures **3** and **4** are also isomorphous, but without cocrystallized solvent.

Calculations. AOM calculations were performed using the AOMX program.[45] DFT calculations were performed using the Gaussian 09[49] package installed on an AMD Opteron G34 12 core server. Two different unrestricted hybrid density functionals, B3LYP (Becke, 3-parameter, Lee−Yang−Parr)[50] and PBE1PBE (Perdew, Burke, and Ernzerhof with 25% exchange weighting),[51] were employed for all calculations. A third hybrid density functional M062X,[63] was explored initially; however, it gave unreasonable results for the electronic structure of the metal center and was not pursued further. In all models, the phenyl groups of Tp^{Ph2} were replaced with methyl groups (Tp*), since these substituents do not affect the overall geometry and hence the metal−halogen interactions. Initial coordinates were obtained from the crystal structures, and the phenyl groups on Tp ligands were modified to methyl groups using DS Viewer Pro (Accelrys). Two-step calculations were conducted to obtain the lowest energy optimized structures. First, single point energies (SPE) were calculated using the valence triple-ζ basis set (6-311G(d))[78] for all atoms. Second, the wave functions generated from SPE calculations were used as a starting point for the geometry optimizations. All models were optimized with added polarization and diffuse functions: 6-311+G(d) for all atoms, and 6-311++G(d) for halogens to obtain improved electronic structures. Tight convergence criteria were used during all optimizations. To estimate the metal−halogen interactions in complexes Tp*Co(2,6-dcp) and Tp*Ni(2,6-dcp), the M−O1−C46$_{phen}$−C47$_{phen}$ dihedral angle in the optimized structure was rotated by 15° increments up to 90°, and these modified models were reoptimized by fixing the dihedral angles at that particular value. Khon-Sham orbitals were analyzed using Gaussview 5 containing Gaussian utilities programs. Mulliken orbital contributions[52−55] from the PBE1PBE calculations with a smaller basis set (6-311G(d)) were analyzed with AOMix.[56,57] Mayer bond orders[58−61] and Wiberg and Löwdin bond indices[62] were determined with AOMix from the Gaussian calculations with the 6-311G basis set. Larger basis sets were found to give unphysical values with all three bond order methods. To examine the phenolate-O to metal charge-transfer transitions, time dependent DFT (TD-DFT) calculations[79] were performed with B3LYP using the geometries obtained from the PBE1PBE calculations. 60 excited states were calculated in each case. Very similar results were also obtained using the B3LYP geometry-optimized structures.

■ ASSOCIATED CONTENT

Ⓢ Supporting Information

Crystallographic data are given in CIF format. Selected geometric data, Wiberg and Löwdin bond orders, optimized energies, and optimized coordinates for the Tp*Co(2,6-dcp) and Tp*Ni(2,6-dcp) models from DFT calculations are provided in Tables S1−S10. Other experimental and computational results are given in Figures S1−S5. This material is available free of charge via the Internet at http://pubs.acs.org.

■ AUTHOR INFORMATION

Corresponding Authors

*E-mail: machonte@whitman.edu.

*E-mail: patrick.holland@yale.edu.

Present Address

[§]Department of Chemistry, Yale University, New Haven, CT 06520.

Notes

The authors declare no competing financial interest.

■ ACKNOWLEDGMENTS

This research was supported by grants from the National Science Foundation (CHE-0951999 to T.E.M. and CHE-0911314 to P.L.H.). The purchase of the 400 MHz Bruker Avance III NMR spectrometer was supported by a grant from the National Science Foundation (MRI-0922775). Analytical data from the University of Rochester used the CENTC Elemental Analysis Facility, funded by NSF CHE-0650456.

■ REFERENCES

(1) *Reregistration Eligibility Decision for Pentachlorophenol*; U.S. Environmental Protection Agency, Office of Pesticide Programs: Arlington, VA, 2008; EPA 739-R-008.

(2) Copley, S. D. *Trends Biochem. Sci.* **2000**, *25*, 261−265.

(3) Ohtsubo, Y.; Miyauchi, K.; Kanda, K.; Hatta, T.; Kiyohara, H.; Senda, T.; Nagata, Y.; Mitsui, Y.; Takagi, M. *FEBS Lett.* **1999**, *459*, 395−398.

(4) Xu, L.; Resing, K.; Lawson, S. L.; Babbitt, P. C.; Copley, S. D. *Biochemistry* **1999**, *38*, 7659−7669.

(5) Xun, L.; Bohuslavek, J.; Cai, M. *Biochem. Biophys. Res. Commun.* **1999**, *266*, 322−325.

(6) Machonkin, T. E.; Holland, P. L.; Smith, K. N.; Liberman, J. S.; Dinescu, A.; Cundari, T. R.; Rocks, S. S. *J. Biol. Inorg. Chem.* **2010**, *15*, 291−301.

(7) Lipscomb, J. D. *Curr. Opin. Struct. Biol.* **2008**, *18*, 644−649.

(8) Vaillancourt, F. H.; Bolin, J. T.; Eltis, L. D. *Crit. Rev. Biochem. Mol. Biol.* **2006**, *41*, 241−267.

(9) Hayes, R. P.; Green, A. R.; Nissen, M. S.; Lewis, K. M.; Xun, L.; Kang, C. *Mol. Microbiol.* **2013**, *88*, 523−536.

(10) Bartels, I.; Knackmuss, H.-J.; Reineke, W. *Appl. Environ. Microbiol.* **1984**, *47*, 500−505.

(11) Cerdan, P.; Wasserfallen, A.; Rekik, M.; Timmis, K. N.; Harayama, S. *J. Bacteriol.* **1994**, *176*, 6074−6081.

(12) Dai, S.; Vaillancourt, F. H.; Maaroufi, H.; Drouin, N. M.; Neau, D. B.; Snieckus, V.; Bolin, J. T.; Eltis, L. D. *Nat. Struct. Biol.* **2002**, *9*, 934−939.

(13) Vaillancourt, F. H.; Labbé, G.; Drouin, N. M.; Fortin, P. D.; Eltis, L. D. *J. Biol. Chem.* **2002**, *277*, 2019−2027.

(14) Machonkin, T. E.; Doerner, A. E. *Biochemistry* **2011**, *50*, 8899−8913.

(15) Rocks, S. S.; Brennessel, W. W.; Machonkin, T. E.; Holland, P. L. *Inorg. Chem.* **2010**, *49*, 10914−10929.

(16) Kuz'mina, L. G. *Russ. J. Coord. Chem.* **1999**, *25*, 599−617.

(17) Meyer, R.; Gagliardi, J.; Wulfsberg, G. *J. Mol. Struct.* **1983**, *111*, 311−316.

(18) Wulfsberg, G.; Yanisch, J.; Meyer, R.; Bowers, J.; Essig, M. *Inorg. Chem.* **1984**, *23*, 715−719.

(19) Richardson, M. F.; Wulfsberg, G.; Marlow, R.; Zaghonni, S.; McCorkle, D.; Shadid, K.; Gagliardi, J., Jr.; Farris, B. *Inorg. Chem.* **1993**, *32*, 1913−19.

(20) Wulfsberg, G. P., Nuclear Quadrupole Resonance (NQR) Spectroscopy. In *Applications of Physical Methods to Inorganic and Bioinorganic Chemistry*, Scott, R. A., Lukehart, C. M., Eds.; John Wiley & Sons: Chichester, U.K., 2007; pp 385−399.

(21) Orpen, A. G.; Brammer, L.; Allen, F. H.; Kennard, O.; Watson, D. G.; Taylor, R. *J. Chem. Soc., Dalton Trans.* **1989**, S1−S83.

(22) Cingi, M. B.; Lanfredi, A. M. M.; Tiripicchio, A.; Reedijk, J.; van Landschoot, R. *Inorg. Chim. Acta* **1980**, *39*, 181−186.

(23) Simonov, Y. A.; Dvorkin, A. A.; Matuzenko, G. S.; Yampol'skaya, M. A.; Gifeisman, T. S.; Gerbeleu, N. V.; Malinovskii, T. I. *Russ. J. Coord. Chem.* **1984**, *10*, 1247−52.

(24) Simonov, Y. A.; Matuzenko, G. S.; Botoshanskii, M. M.; Yampol'skaya, M. A.; Gerbeleu, N. V.; Malinovskii, T. I. *Russ. J. Inorg. Chem.* **1982**, *27*, 231−234.

(25) Basturkmen, M.; Kisakurek, D.; Driessen, W.; Gorter, S.; Reedijk, J. *Inorg. Chim. Acta* **1998**, *271*, 19−23.
(26) Camurlu, P.; Yilmaz, A.; Tatar, L.; Kisakurek, D.; Ulku, D. *Cryst. Res. Technol.* **2005**, *40*, 271−276.
(27) Ulku, D.; Tahir, M. N.; Kesici, N.; Isci, H.; Kisakurek, D. *Z. Kristallogr.-New Cryst. Struct.* **1997**, *212*, 493−494.
(28) Trofimenko, S. *Chem. Rev.* **1993**, *93*, 943−980.
(29) Kitajima, N.; Tolman, W. B. *Prog. Inorg. Chem.* **1995**, *43*, 419−531.
(30) Pettinari, C.; Santini, C., Polypyrazolylborate and Scorpionate Ligands. In *Comprehensive Coordination Chemistry II*; McCleverty, J. A., Meyer, T. J., Eds.; Elsevier Pergamon: Amsterdam, 2004; Vol. *1*, pp 159−210.
(31) Kitajima, N.; Fujisawa, K.; Fujimoto, C.; Moro-oka, Y.; Hashimoto, S.; Kitagawa, T.; Toriumi, K.; Tatsumi, K.; Nakamura, A. *J. Am. Chem. Soc.* **1992**, *114*, 1277−1291.
(32) Ito, M.; Amagai, H.; Fukui, H.; Kitajima, N.; Moro-Oka, Y. *Bull. Chem. Soc. Jpn.* **1996**, *69*, 1937−1945.
(33) Deb, T.; Rohde, G. T.; Young, V. G.; Jensen, M. P. *Inorg. Chem.* **2012**, *51*, 7257−7270.
(34) Baum, A. E.; Park, H.; Wang, D. N.; Lindeman, S. V.; Fiedler, A. T. *Dalton Trans.* **2012**, *41*, 12244−12253.
(35) Bittner, M. M.; Kraus, D.; Lindeman, S. V.; Popescu, C. V.; Fiedler, A. T. *Chem.—Eur. J.* **2013**, *19*, 9686−9698.
(36) Bittner, M. M.; Lindeman, S. V.; Fiedler, A. T. *J. Am. Chem. Soc.* **2012**, *134*, 5460−5463.
(37) Harding, D. J.; Harding, P.; Adams, H.; Tuntulani, T. *Inorg. Chim. Acta* **2007**, *360*, 3335−3340.
(38) Harding, D. J.; Harding, P.; Daengngern, R.; Yimklan, S.; Adams, H. *Dalton Trans.* **2009**, 1314−1320.
(39) Addison, A. W.; Rao, T. N.; Reedijk, J.; Vanrijn, J.; Verschoor, G. C. *J. Chem. Soc., Dalton Trans.* **1984**, 1349−1356.
(40) Bondi, A. *J. Phys. Chem.* **1964**, *68*, 441−451.
(41) Mantina, M.; Chamberlin, A. C.; Valero, R.; Cramer, C. J.; Truhlar, D. G. *J. Phys. Chem. A* **2009**, *113*, 5806−5812.
(42) Auffinger, P.; Hays, F. A.; Westhof, E.; Ho, P. S. *Proc. Natl. Acad. Sci. U.S.A.* **2004**, *101*, 16789−16794.
(43) Bertini, I.; Luchinat, C.; Parigi, G. *Solution NMR of Paramagnetic Molecules*; Elsevier: Amsterdam, 2001.
(44) Gorelsky, S. I.; Basumallick, L.; Vura-Weis, J.; Sarangi, R.; Hodgson, K. O.; Hedman, B.; Fujisawa, K.; Solomon, E. I. *Inorg. Chem.* **2005**, *44*, 4947−4960.
(45) Adamsky, H. *AOMX*; Institut für Theoretische Chemie, Heinrich-Heine-Universität: Düsseldorf, Germany, 1996.
(46) Krzystek, J.; Swenson, D. C.; Zvyagin, S. A.; Smirnov, D.; Ozarowski, A.; Telser, J. *J. Am. Chem. Soc.* **2010**, *132*, 5241−5253.
(47) Holm, R. H.; Kennepohl, P.; Solomon, E. I. *Chem. Rev.* **1996**, *96*, 2239−2314.
(48) Desrochers, P. J.; Telser, J.; Zvyagin, S. A.; Ozarowski, A.; Krzystek, J.; Vicic, D. A. *Inorg. Chem.* **2006**, *45*, 8930−8941.
(49) Frisch, M. J.; Trucks, G. W.; Schlegel, H. B.; Scuseria, G. E.; Robb, M. A.; Cheeseman, J. R.; Scalmani, G.; Barone, V.; Mennucci, B.; Petersson, G. A.; Nakatsuji, H.; Caricato, M.; Li, X.; Hratchian, H. P.; Izmaylov, A. F.; Bloino, J.; Zheng, G.; Sonnenberg, J. L.; Hada, M.; Ehara, M.; Toyota, K.; Fukuda, R.; Hasegawa, J.; Ishida, M.; Nakajima, T.; Honda, Y.; Kitao, O.; Nakai, H.; Vreven, T.; J. A. Montgomery, J.; Peralta, J. E.; Ogliaro, F.; Bearpark, M.; Heyd, J. J.; Brothers, E.; Kudin, K. N.; Staroverov, V. N.; Kobayashi, R.; Normand, J.; Raghavachari, K.; Rendell, A.; Burant, J. C.; Iyengar, S. S.; Tomasi, J.; Cossi, M.; Rega, N.; Millam, J. M.; Klene, M.; Knox, J. E.; Cross, J. B.; Bakken, V.; Adamo, C.; Jaramillo, J.; Gomperts, R.; Stratmann, R. E.; Yazyev, O.; Austin, A. J.; Cammi, R.; Pomelli, C.; Ochterski, J. W.; Martin, R. L.; Morokuma, K.; Zakrzewski, V. G.; Voth, G. A.; Salvador, P.; Dannenberg, J. J.; Dapprich, S.; Daniels, A. D.; Farkas, Ö.; Foresman, J. B.; Ortiz, J. V.; Cioslowski, J.; Fox, D. J. *Gaussian 09*, revision C 01; Gaussian, Inc.: Wallingford, CT, 2010.
(50) Becke, A. D. *J. Chem. Phys.* **1993**, *98*, 5648−5652.
(51) Adamo, C.; Barone, V. *J. Chem. Phys.* **1999**, *110*, 6158−6170.
(52) Mulliken, R. S. *J. Chem. Phys.* **1955**, *23*, 1833−1840.
(53) Mulliken, R. S. *J. Chem. Phys.* **1955**, *23*, 1841−1846.
(54) Mulliken, R. S. *J. Chem. Phys.* **1955**, *23*, 2338−2342.
(55) Mulliken, R. S. *J. Chem. Phys.* **1955**, *23*, 2343−2346.
(56) Gorelsky, S. I. *AOMix*, 6.81; University of Ottawa: Ottawa, Ontario, 2013.
(57) Gorelsky, S. I.; Lever, A. B. P. *J. Organomet. Chem.* **2001**, *635*, 187−196.
(58) Mayer, I. *Chem. Phys. Lett.* **1983**, *97*, 270−274.
(59) Mayer, I. *Theor. Chim. Acta* **1985**, *67*, 315−322.
(60) Mayer, I. *Int. J. Quantum Chem.* **1986**, *29*, 73−84.
(61) Mayer, I. *Int. J. Quantum Chem.* **1986**, *29*, 477−483.
(62) Natiello, M. A.; Medrano, J. A. *Chem. Phys. Lett.* **1984**, *105*, 180−182.
(63) Zhao, Y.; Truhlar, D. G. *J. Chem. Theory Comput.* **2007**, *3*, 289−300.
(64) *CRC Handbook of Chemistry and Physics*, 90th ed.; CRC Press: Boca Raton, FL, 2009.
(65) Lommerse, J. P. M.; Stone, A. J.; Taylor, R.; Allen, F. H. *J. Am. Chem. Soc.* **1996**, *118*, 3108−3116.
(66) Metrangolo, P.; Meyer, F.; Pilati, T.; Resnati, G.; Terraneo, G. *Chem. Commun.* **2008**, 1635−1637.
(67) Imai, Y. N.; Inoue, Y.; Nakanishi, I.; Kitaura, K. *Protein Sci.* **2008**, *17*, 1129−1137.
(68) Matter, H.; Nazare, M.; Gussregen, S.; Will, D. W.; Schreuder, H.; Bauer, A.; Urmann, M.; Ritter, K.; Wagner, M.; Wehner, V. *Angew. Chem., Int. Ed. Engl.* **2009**, *48*, 2911−2916.
(69) Perrin, C. L.; Nielson, J. B. *Annu. Rev. Phys. Chem.* **1997**, *48*, 511−544.
(70) Ammann, C.; Meier, P.; Merbach, A. E. *J. Magn. Reson.* **1982**, *46*, 319−321.
(71) Harris, D. C. *J. Chem. Educ.* **1998**, *75*, 119−121.
(72) Since complexes **1** and **2** were both colorless, and the UV−vis-NIR spectrum of **2** showed only a shoulder at ∼360 nm (see below), the UV−vis-NIR spectrum of **1** was not obtained.
(73) Sheldrick, G. M. *SADABS*, 2008/1; University of Göttingen: Göttingen, Germany, 2008.
(74) *SAINT*, 7.60A; Bruker AXS: Madison, WI, 2008.
(75) Altomare, A.; Burla, M.; Cascarano, G. L.; Giacovazzo, C.; Guagliardi, A.; Moliterni, A. G. G.; Polidori, G.; Spagna, R. *SIR97*; Istituto di Cristallografia: CNR Bari, Italy, 1999.
(76) Sheldrick, G. M. *Acta Crystallogr. A* **2008**, *64*, 112−122.
(77) Spek, A. L. *Acta Crystallogr. D* **2009**, *65*, 148−155.
(78) Schäfer, A.; Horn, H.; Ahlrichs, R. *J. Chem. Phys.* **1992**, *97*, 2571−2577.
(79) Stratmann, R. E.; Scuseria, G. E.; Frisch, M. J. *J. Chem. Phys.* **1998**, *109*, 8218−8224.